LABORATORI NAZIONALI DI FRASCATI
SIS – Pubblicazioni

LNF-95/052 (P)
28 Settembre 1995

The WiZard/CAPRICE Silicon-Tungsten Calorimeter

M. Bocciolini, F. Celletti, N. Finetti, M. Grandi, P. Papini, A. Perego, S. Piccardi, P. Spillantini
Dipartimento di Fisica dell'Università di Firenze and Sezione INFN di Firenze, Italy

V. Bidoli, M. Candusso, M. Casolino, M.P. De Pascale, A. Morselli, P. Picozza, R. Sparvoli
Dipartimento di Fisica dell'Università "Tor Vergata", Roma and Sezione INFN di Roma II, Roma, Italy

G. Basini, G. Mazzenga, M. Ricci
Laboratori Nazionali INFN, Frascati, Italy

F.Bronzini
Dipartimento di Fisica dell'Università "La Sapienza", Roma and Sezione INFN di Roma, Roma, Italy

G. Barbiellini, M. Boezio, U. Bravar, F. Fratnik, P. Schiavon, A. Vacchi, N. Zampa
Dipartimento di Fisica dell'Università, Trieste and Sezione INFN di Trieste, Trieste, Italy

Abstract

A silicon-tungsten calorimeter has been developed to be flown in the WiZard/CAPRICE balloon borne experiment to measure the flux of antiprotons, positrons and light nuclei in the cosmic radiation. The calorimeter is composed of 8 x, y silicon sampling planes [active area (48x48) cm^2] interleaved with 7 tungsten absorbers (7 radiation lengths); it provides the topology of the interacting events together with an independent measurement of the deposited energy. Details of the front-end electronics and of the read-out system are given and the overall performances during pre-flight ground operations are described as well.

PACS.: 29.40; 95.55

Accepted by Nucl. Instr. & Method in Phys. Res.

1 – Introduction

The application of silicon detectors as active layers for sampling calorimeters is a well-established technique in high-energy physics experiments. The main features and advantages of such detectors as stability, linearity, low-voltage operation, no need of gas, allow to extend their utilization also to cosmic ray experiments conducted in space [1]. The calorimeter here described is an upgraded version carried out for a balloon flight, named CAPRICE (Cosmic Antiparticle Ring Imaging Cherenkov Experiment), to measure the flux of low-energy antiprotons, positrons and light isotopes in the cosmic radiation. A first version of the calorimeter with a different read-out system was flown in 1993 in an experiment to measure the flux of high-energy electrons and positrons (flight named TS93) [2].

Limitations in weight and power consumption are the most severe constraints to be considered for the design and construction of this instrument: as a consequence, its depth is insufficient for the full containment of high-energy electromagnetic showers. However, previous prototype tests performed at CERN PS beams [3,4,5] have shown that the granularity and the energy resolution of the silicon detectors make them capable to measure the transverse and longitudinal shower profiles and to track the particles with high accuracy. This instrument fulfills its task as a particle identifier.

The experimental set-up of the payload for the balloon flight is shown in Fig. 1. A superconducting magnet, placed at the side of a tracking system, made of Multiwire Proportional and Drift Chambers, constitutes the spectrometer for the measurement of the momentum of the incident particles and nuclei [6,7].

A set of plastic scintillators, installed at the upper and lower edges of the tracking system, is used to provide both the trigger of the experiment and the time of flight (TOF) information with a resolution of 400 ps over ≈ 120 cm of path length: this system also provides an energy loss (dE/dx) measurement over a thickness of 1+1 cm of the plastic scintillators.

Placed at the top of the apparatus is a Ring Imaging Cherenkov (RICH) counter [8,9] for particle and isotope identification through Cherenkov angle measurement.

The calorimeter is located below the tracking system; it operates in conjuction with the RICH to identify particles and nuclei by distinguishing between hadronic and electromagnetic showers and by measuring the energy released in each sampling layer.

2 – The Detector

The calorimeter, shown in Fig. 2, is composed of 8 sensitive silicon planes, with an active area of (48x48) cm^2, interleaved with 7 layers of tungsten absorbers, each layer one radiation length (X_0) thick. Taking into account all the material the calorimeter has a total of 7.2 X_0's and 0.33 interaction lengths.

A single plane is a matrix of 8x8 silicon modules mounted on a G10 motherboard. Each module is composed of two silicon detectors, 380 μm thick, having an active area of (6 x 6) cm^2, divided in 16 strips, 3.6 mm wide. They are mounted back to back with perpendicular strips to provide double coordinate (x-y) read-out, as shown in Fig. 3a. The strips of each detector are daisy-chained longitudinally to form one single strip 48 cm long. One plane has 256 channels (128x + 128y), fed into two sets of eight front-end modules, 16 channels each, for x and y coordinates as illustrated in Fig. 3b. The whole calorimeter has 2048 channels. Details about the characteristics of the silicon detectors, the assembly of the module, the plane arrangement and the checks step by step are published, together with the results of the successive tests, in Refs. [3-5].

The flight configuration has been designed in order to place in the same mechanical structure all the required servicing devices. The potographies in Fig. 4 show the complete

arrangement of the calorimeter for ground, stand-alone tests (4a) and once installed in the payload (4b). This arrangement includes a water cooling box and a dedicated CAMAC crate. The crate contains all the read-out modules (see below) and two lithium battery power supply modules used to polarize the silicon planes: voltages can vary (from 60 V to 110 V) according to the different kind and thickness of the silicon detectors employed. In such a way it is possible to turn independently on and off and to costantly monitor each plane through simple software commands.

3 – Data Acquisition System

The data acquisition system is organized as schematically shown in Fig. 5 for one plane. The trigger signal enables a driver to start the read-out sequence: a command sent to every channel latches the detector signals, which are then multiplexed on a single output for each plane.

Each output is fed into a separate conversion unit, where analog to digital conversion, optional zero skip, data formatting and buffering are performed; therefore, all the planes are read in parallel. The data are then processed by the payload computer.

3.1 Front-end

The basic front-end consists of a 16-channel module (Fig. 3b), providing the analog circuitry for the charge amplification and the sample-and-hold of each channel, as well as the logic to drive the sample-and-hold itself and the multiplexed output. Sixteen front-end modules are needed to handle the signals from the detectors of each plane for both coordinates. A scheme is shown in Fig. 6. Each channel features a charge preamplifier, with a JFET in the input stage and a semi-gaussian shaping network with a peaking time of 7 μs.

The semi-Gaussian shaping is an usual convenient circuital compromise for a "time invariant filter" which we have chosen because of the random character of the incoming data. Concerning the peaking time, the following points have been taken into account:

a) The relationship between noise and shaping time has the form:

$$\overline{ENC}^2 = A/\tau + B + C\tau I_L$$

where $\overline{ENC}^2$ (Equivalent Noise Charge) is the r.m.s. value of electronic fluctuations, A, B, C are constants depending on the chosen shape, on the JFET input stage parameters and on the temperature, respectively, τ is the peaking time and I_L the leakage current of the detector. A working value of τ may be drawn by this relationship as it is shown in Fig. 7 where $\overline{ENC}^2$ for different contributions to the noise is plotted as a function of τ itself.

b) The expected rate is very low (~400 Hz at balloon floating altitude), so that pile-up problems are quite negligible.

c) During the peaking time, it is possible to perform some elaboration before starting the read-out (first level trigger).

d) For a given dynamic range, the longer is the shaping time, the smaller is the power required by the analog circuitry.

Once the data have been latched into the analog memories, the read-out circuitry multiplexes the 16 channels onto a single output. A post-amplifier is provided for each channel so that the signal may be read at two different amplification gains (x16 and x1), with the maximum output level (3.5 V) corresponding to 28 and 450 mip (minimum ionizing particles), respectively. This feature has proved to be very useful both in preventing signals of low-energy events from being further deteriorated by noise picked-up after the front-end, and in allowing a

broader dynamic range.

A bipolar output signal, whose amplitude is proportional to the total charge injected into the 16 channels, is also provided. The zero-crossing of this output line, which has no correlation with the sample-and-hold and read-out logic, may be used as a timing signal for auto-trigger purposes.

The physical structure of each front-end module consists of three tightly stacked boards with discrete, surface mounted, elements, with total dimensions 1.1 cm x 6 cm x 15 cm and 80 g weight. To allow for fast replacing, the modules of a plane are simply plugged onto two connection boards (x and y channels), located on two adjacent sides of the sensitive plane. At the corner between these two sides an interface triangular board (see Fig. 2) is placed to provide the circuitry to distribute and collect the signals and the silicon detector's polarization voltage, with proper impedance matching. To allow for the most compact configuration, the connection and corner boards of adjacent planes are mounted on opposite sides.

The total power consumption attributed to the front-end electronics is 83 W.

3.2 – Read-out and buffering units

A single CAMAC read-out driver provides the signals needed to perform the multiplexed read-out of all the front-end modules upon receipt of a trigger signal. A gate pulse is sent to the conversion units to start their operation causing the analog input to be sampled by an 8-bit ADC. The address of the actual channel is simultaneously put on a bus that connects all the conversion units. All the 256 channels of a plane are scanned at 1 MHz rate, in two subsequent cycles for the two amplifications. Thus, a complete read-out sequence takes 512 μs.

The conversion and buffering units, standard CAMAC modules*, one for each calorimeter plane, also perform an optional zero-skip of the data and store them into buffer memories that are accessed by the controlling computer in the final stage of the read-out. The digitized data are combined with the strip address, latched simultaneously, and formatted with the converted datum into a 16-bit word. The read-out driver notifies the conversion units of the switching from xl to x16 gain and of the completion of the acquisition cycle, and, correspondingly, separation words are stored into memory. A latched trigger number is also added to the data pertaining to each event. Two 16-kword memory buffers are provided for each conversion unit, so that one of them may be loaded with new data while the other is being read by the controlling computer.

The power cosumption related to the CAMAC system is 98 W which, together with the front-end consumption previously quoted, gives a total of 181 W for the whole calorimeter.

4 – Mechanical assembly

4.1– Calorimeter box

In order to be qualified for a balloon flight, the mechanical structure of the calorimeter, as for any other detector of the Payload, has been designed to support 10 g's vertically and 5 g's horizontally. Moreover, the calorimeter has to hold the weight of the above detectors (mainly the tracking system) and of part of the magnet. Therefore, a solid, compact and as less heavy as possible structure has been designed.

A photography of the bare mechanical structure is shown in Fig. 8; two main parts are described: internal and external.

The basic element of the internal structure is an anodized aluminum honeycomb base-plate

---

* Developed and built by CAEN, Italy

with four steel posts (columns) which follow the mechanical structure of the tracking system placed above the calorimeter. A series of threaded columns made of an aluminum alloy (anticorodal), 5 mm diameter, are welded on each side of the base-plate to allow the assembly of the silicon planes, the tungsten layers, the preamplifiers and the read-out corner boards in a modular way.

An aluminum box, 2 mm thick, covers and seals all the internal structure to provide thermical insulation, protection from light and to allow for nitrogen flowing to keep the environment dry. An internal top cover tightly compresses the entire structure thus preventing from any kind of oscillation (mainly in the central part) and distributing the stresses over the four posts. This cover is made of two parts: i) an aluminum alloy (Ergal) frame 30 mm thick bolted to the four posts and covering the side area of the plane corresponding to the preamplifiers' connection boards; ii) a plexiglas plate 20 mm thick, covering and protecting all the active area of the first top silicon plane.

The external part of the mechanical structure is composed of a base-plate connected to the internal one through the same four steel posts (Fig. 8) In this area are placed the water cooling box, the CAMAC Crate and the servicing boards for the readout power supplies and for the monitoring from ground. The base plate sits on the main bottom structure of the Payload that supports all the stack of detectors. The weight of the whole bare mechanical structure is 85 kg while the weight of the entire calorimeter, including the CAMAC crate and the cooling box filled with water, is 300 kg.

4.2 – Cooling system

It is known that a better performance of the silicon detectors can be achieved if they can work in a cooled environment. Due to the temperature variations inside the Payload during the flight (between 10 °C and 38 °C) an independent cooling system has been designed and carried out for the calorimeter. A first prototype version of this system was tested during the TS93 balloon flight.

The concept is based on the evaporation of water in almost vacuum conditions (about 4 mbar at balloon floating altitude). A vacuum-proof stainless steel (1 mm thick) water box has been designed to be attached below the base-plate of the calorimeter; it has an area of (45 x 45) cm^2 and a height of 12.3 cm (the total capacity is about 25 lt); a photography of the box is displayed in Fig. 9. Four aluminum triangular plates, 2 mm thick, hang from the base-plate of the calorimeter through cylindrical supports and are immersed in the water; this improves the thermal conductivity between the box, the base-plate and the whole calorimeter.

As the pressure inside the Payload is maintained at ~1 atm the near-vacuum conditions in the cooling box are reached by linking it to the outside through a flexible pipeline (3/4" diameter); it goes from the box to a hermetic hole located on the top section of the payload wall. To prevent from any depressurizing hazard an electrovalve (normally open) placed along this line can be quickly operated through a software command from ground if necessary. During ground operations the cooling of the calorimeter is performed by means of an external chiller. The monitoring of the performance of the cooling system, either at ground or during the flight, is accomplished through three sensors that control the water level, the temperature and the pressure inside the box, respectively.

5 – Simulation and performances

Based upon the same technique, silicon calorimeters different only for geometrical arrangements and radiation lengths have been extensively studied by our group through Monte Carlo simulations, beam tests and the previous TS93 balloon flight [2-5].

The CAPRICE flight model has been further investigated through a Monte Carlo simulation program based on the GEANT code [10]. Since the primary objective of the flight is the determination of the antiproton flux at low energies (0.5-5.0 GeV), simulated data have been analysed using a set of cuts giving the highest efficiency in antiproton detection against the electron background. Results in the energy ranges of interest are reported in Table I.

Table I – Monte Carlo results: calculated efficiencies in antiproton detection against electron contamination.

Momentum (GeV/c)	$\bar{p}$ efficiency	e^- contamination on $\bar{p}$
0.5 - 1	(72.0±1.0)%	(4.0±0.3)%
1 - 2	(83.9±0.5)%	(2.2±0.3)%
2 - 3	(92.7±0.4)%	(2.5±0.4)%
3 - 5	(95.1±0.3)%	(1.5±0.3)%

The actual response of the whole calorimeter and its efficiency have been measured with cosmic rays during ground tests triggering with an independent scintillator telescope. In Fig. 10 histograms of the energy deposition in some strips are shown. The first peak is the truncated tail of the pedestal, the second is the Landau shaped energy of minimum ionizing particles; more energetic depositions are distinguishable in its tail. The amplification shown is related to the x16 gain, as one can verify from the saturation of the 256th channel. Pictures of the imaging capability of the calorimeter are given in Fig. 11, where a non interacting particle (a) and an interacting one (b) are shown, respectively.

6 – Conclusions

We have described a silicon-tungsten calorimeter designed for a balloon borne experiment (CAPRICE) to measure the antiproton, positron and light nuclei component in the cosmic rays. Its major task is the separation between e.m. and hadronic showers by topology information and the measurement of the deposited energy.

This instrument is the result of successive phases of preparations and intermediate realizations that have made it possible to achieve a reliable mean of scientific investigation. Besides its specific use on a balloon borne apparatus, it has also been developed as a basic model susceptible of improvements and upgradings for other space activities (i.e. on satellites) within the WiZard program. Here are summarized the most significant features:

a) The construction technique of the silicon detectors has been improved in close collaboration with the industry: for instance, the value of the average leakage currents has been reduced down to 5 nA/cm^2 and the observed behaviour is totally reproducible.
b) The data acquisition system is organized in such a way to avoid any problem of pick-up noise caused by the logic circuitry; indeed, no clock is running when the outputs of the silicon detectors are amplified and sampled.
c) The data formatting identifies each event in the buffers of the conversion units, so that several events can be stored. This feature provides a significant de-randomization and minimizes the computer overhead associated with the start of each read-out operation.
d) The instrument is modular both in the plane layout and in the organization of the data acquisition.
e) The acquisition time for a single event is limited to 512 μs and is totally independent of the number of planes that are read in parallel.

f) Even if weight and volume limitations did not allow to get the full containment of high energy showers, the performances of this detector, either from beam tests or from ground pre-flight checkouts, have shown that particle tracking and identification can be performed with high accuracy.

Full results and flight performances in conjunction with the other detectors of the CAPRICE apparatus will be the object of future publications as far as the data analysis is completed.

Acknowledgements

We wish to thank the staff personnel at Particle Astrophysics Lab of the New Mexico State University, Las Cruces, for their help during the integration and pre-fligfit procedures; in particular we want to remember the late Robert L. Golden, Principal Investigator of the Wizard balloon-borne experiments whose continuous encouragement and tireless perseverance has made this collaboration possible.

The help received by Mr Gianluca Renna and Dr Guido Paoluzi of the University of Tor Vergata, Rome is aknowledged for their thecnical support during the construction of the calorimeter.

References

[1] G.Barbiellini et al., Nuovo Cim. **102B** (1988) 661.
[2] F.Aversa et al., Nucl. Instr. Meth. **A360** (1995) 17.
[3] M.Bocciolini et al., Proc. 3rd Int. Conf. on Calorimetry in High Energy Physics, Corpus Christi, Texas, (1992) p.285.
[4] M.Bocciolini et al., Nucl. Instr. Meth. **A333** (1993) 560.
[5] M.Bocciolini et al., Nucl. Phys. **B32** (1993) 77.
[6] R.L.Golden et al., Nucl. Instr. Meth. **A306** (1991) 366.
[7] M.Hof et al., Nucl. Instr. Meth. **A345** (1994) 561.
[8] P.Carlson et al., Nucl. Instr. Meth. **A343** (1994) 198.
[9] P.Carlson et al., Nucl. Instr. Meth. **A349** (1994) 577.
[10] R.Brun et al., CERN GEANT 3 User's Guide, DD/EE/84-1(1992).

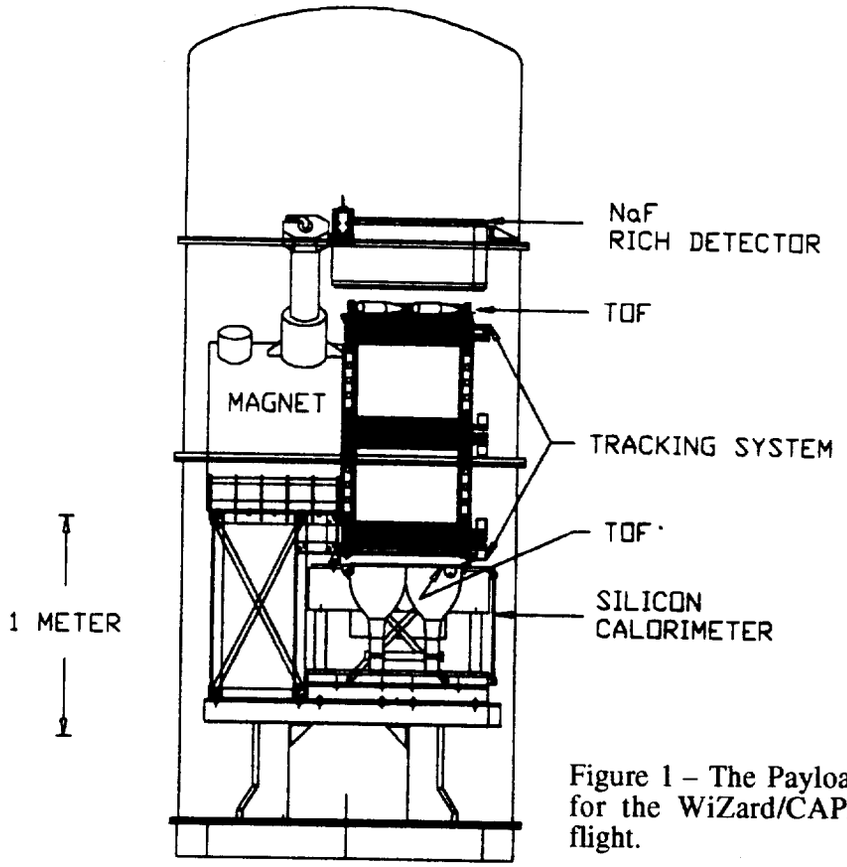

Figure 1 – The Payload arrangement for the WiZard/CAPRICE balloon flight.

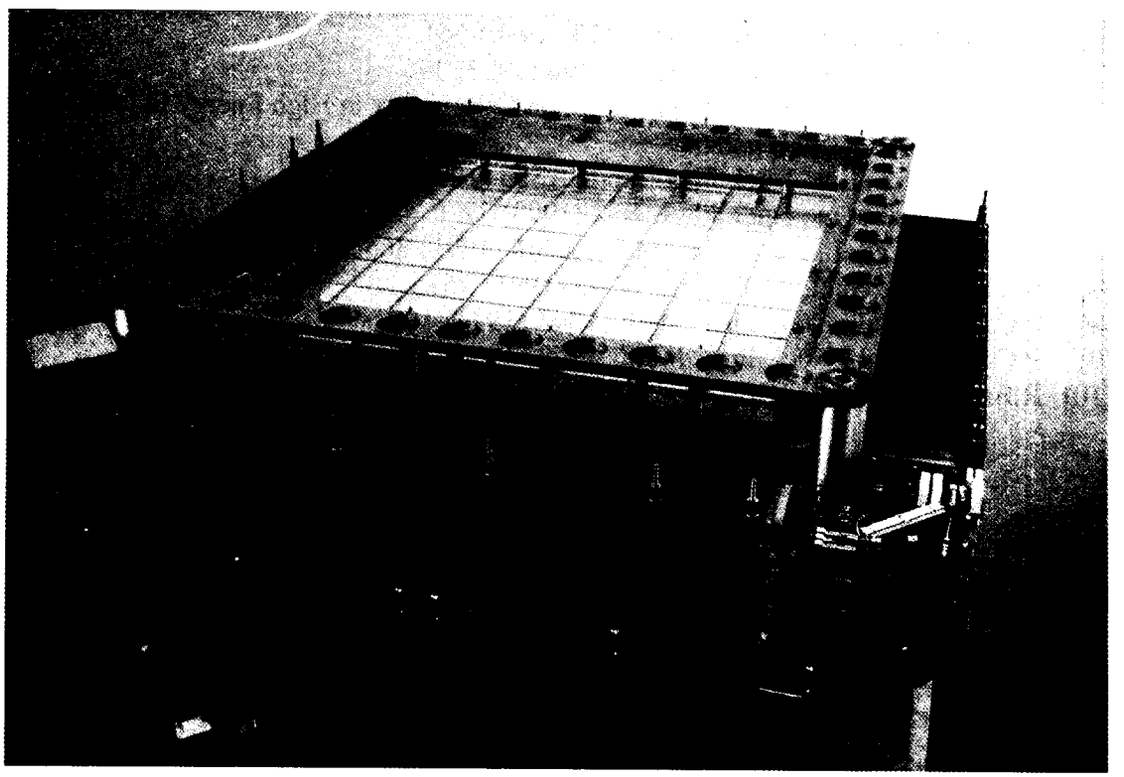

Figure 2 – The calorimeter assembled on its mechanical structure.

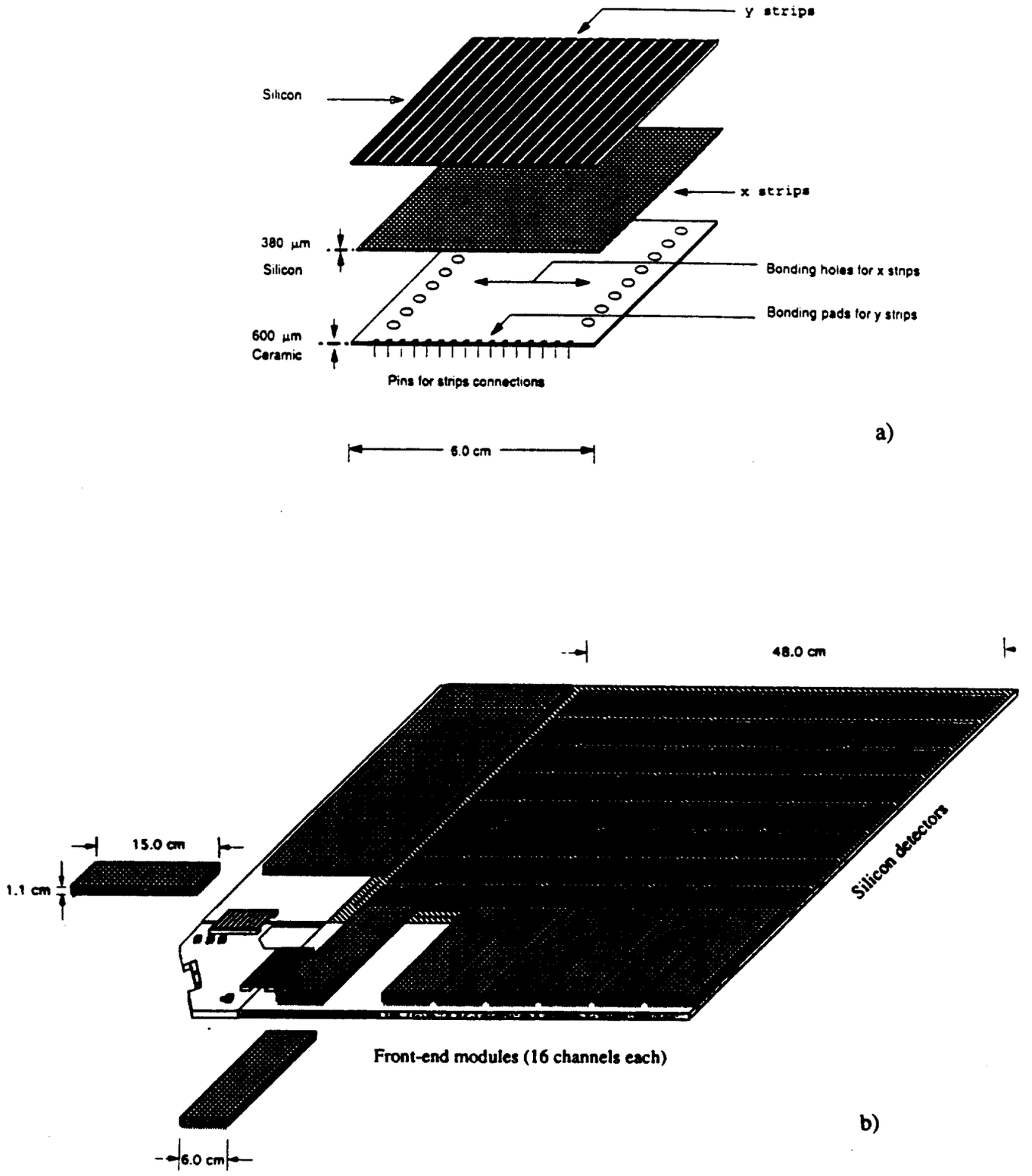

Figure 3 – a) Exploded view of one a single silicon module (x and y coordinates) on its ceramic support; b) the silicon plane arrangement. The 16-channel preamplifier modules are also shown.

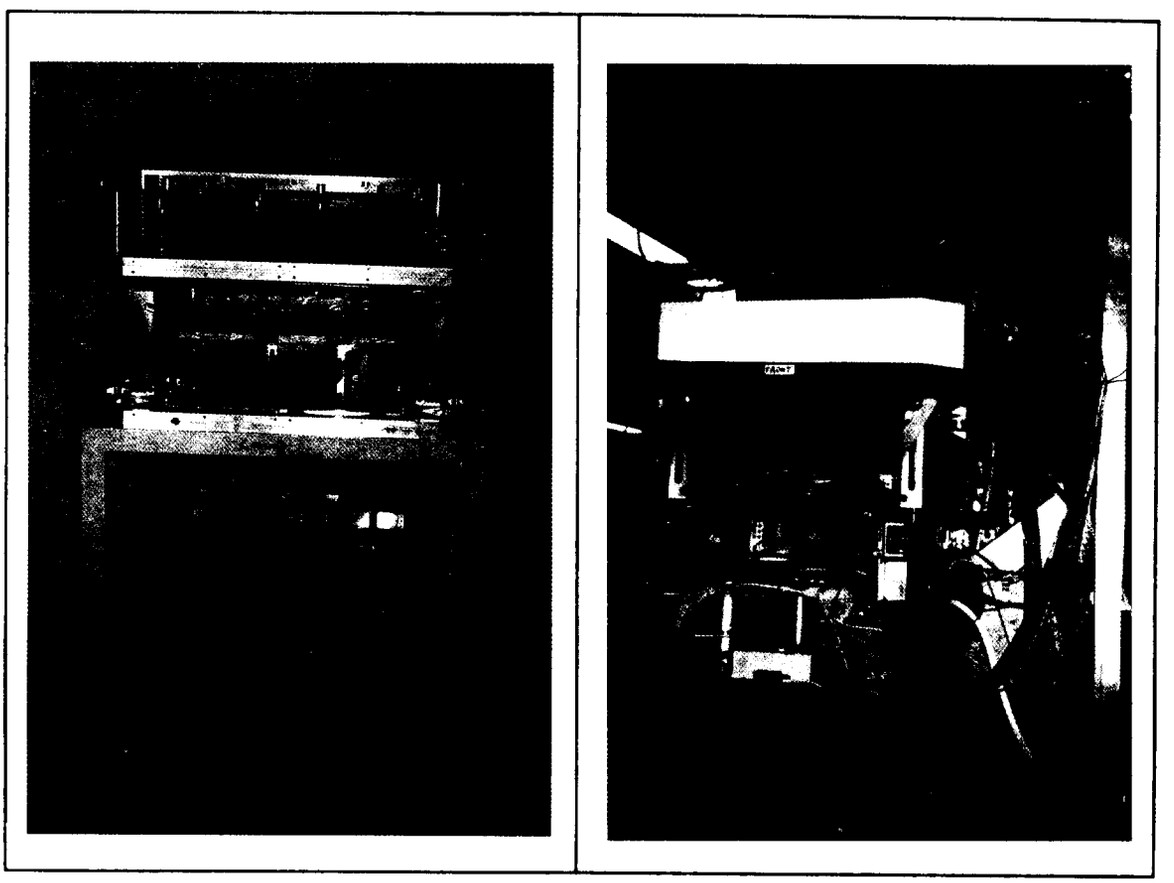

a) b)

Figure 4 – Photographies of the complete arrangement of the calorimeter with its cooling box and the dedicated CAMAC Crate. a): stand-alone configuration without the cover; b) flight configuration in the payload; above the calorimeter stands the superconducting magnet.

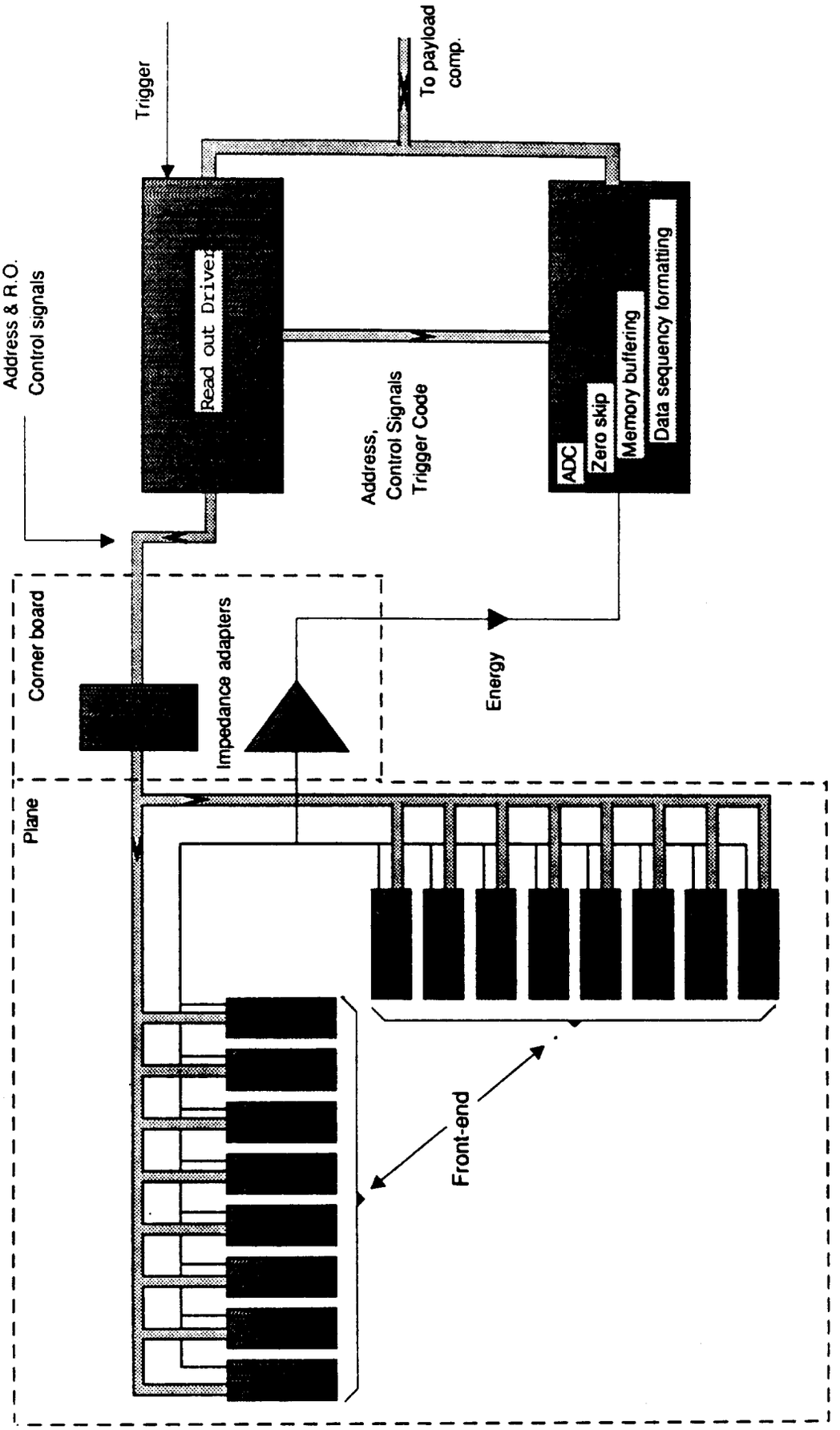

Figure 5 – The organization of the data acquisition system (right side) and the read–out logic for one plane (left side).

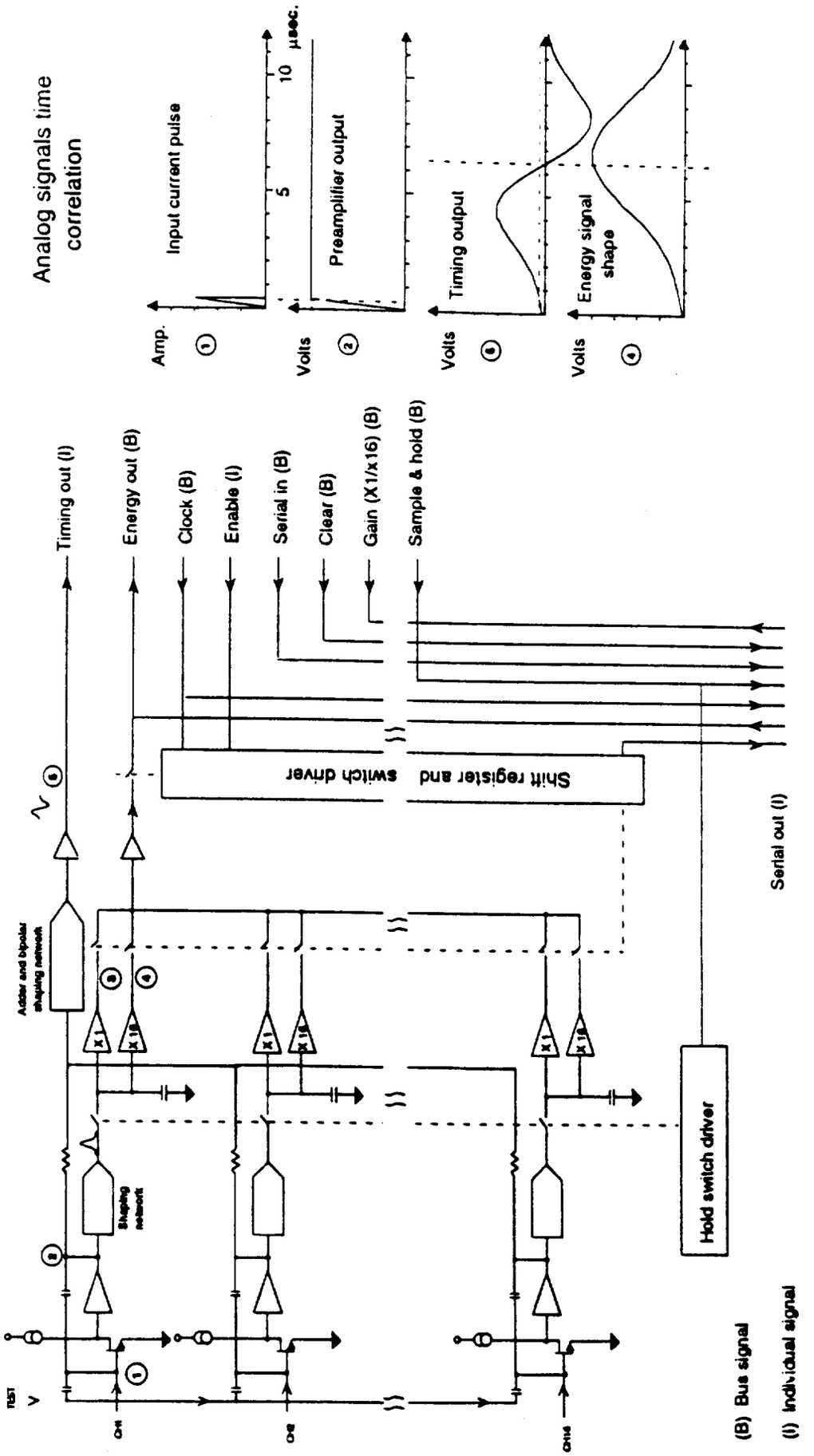

Figure 6 – Front–end schematic diagram for a single 16–channel preamplifier module. The time correlation of some of the analog signals is also shown.

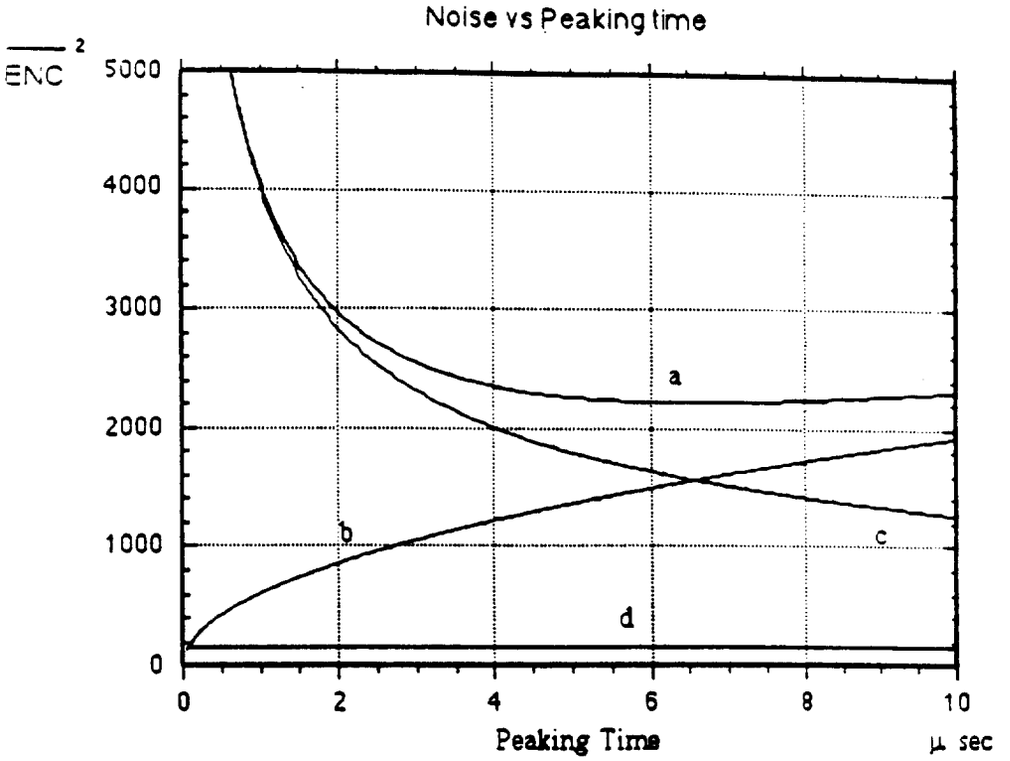

Figure 7 – Front-end electronics: Equivalent Noise Charge (ENC) vs. peaking time. The curves displayed are: a: total noise; b: current noise; c: shot noise; d: 1/f noise. The chosen working point is 7 μs.

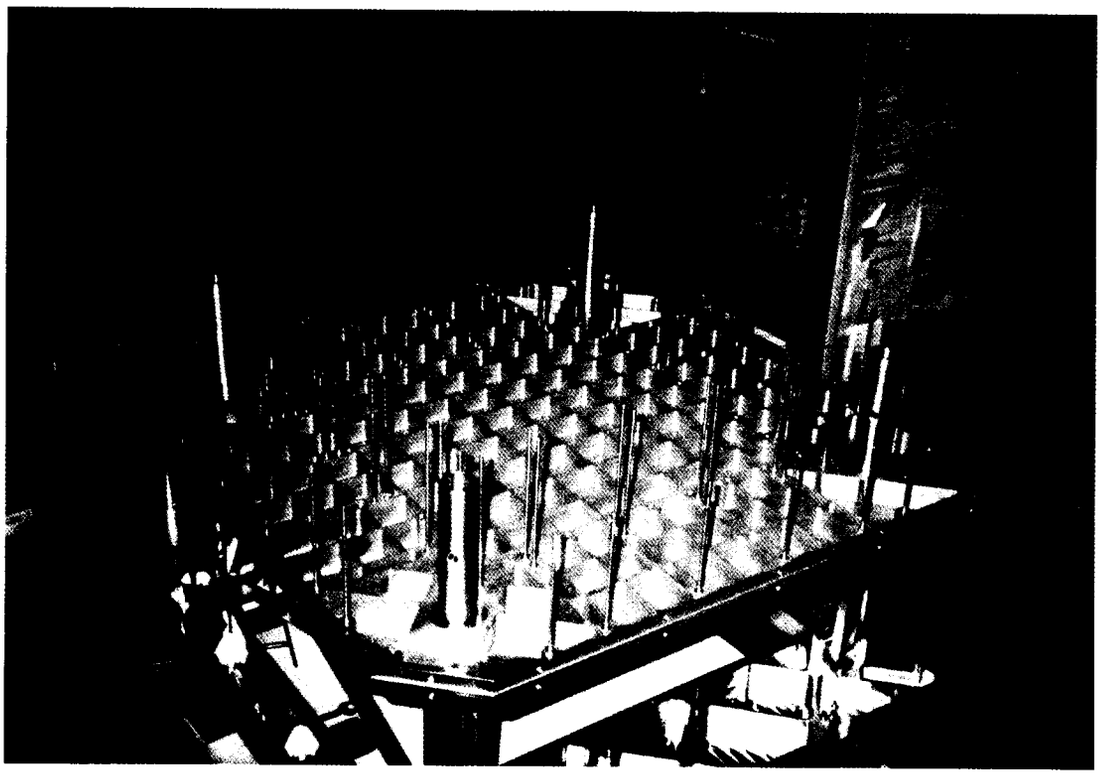

Figure 8 – Photography of the bare mechanical structure showing the honeycomb base-plate with its four steel posts and all the threaded columns for the assembly of the planes (silicon and tungsten) and of the front-end boards.

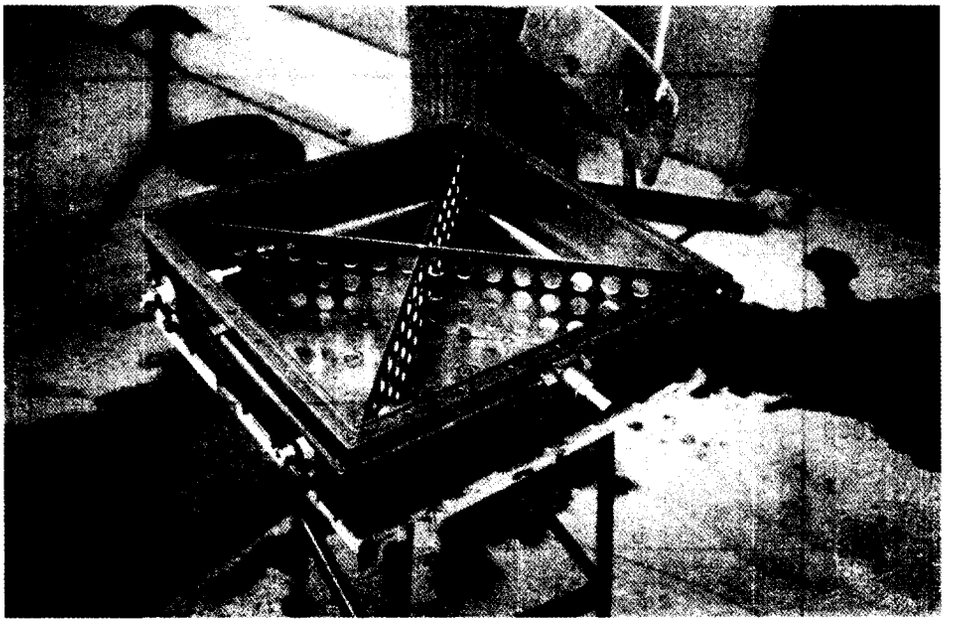

Figure 9 – The water cooling box once removed from the calorimeter: visible is also a copper pipe for the circulation of water cooled by an external chiller.

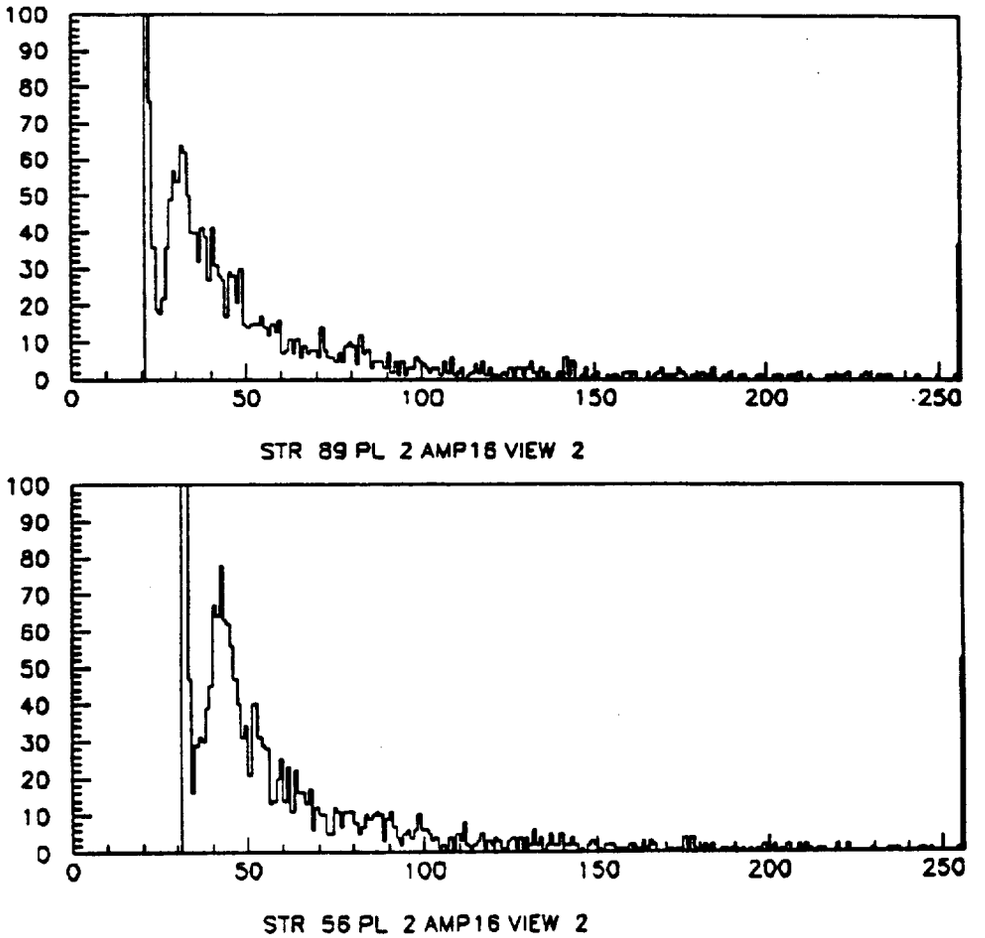

Figure 10 – Histogram of the energy deposited into two different strips. Counts are in arbitrary units while abscissa is in ADC channels. The saturation on the last (256th) ADC channel is also visible.

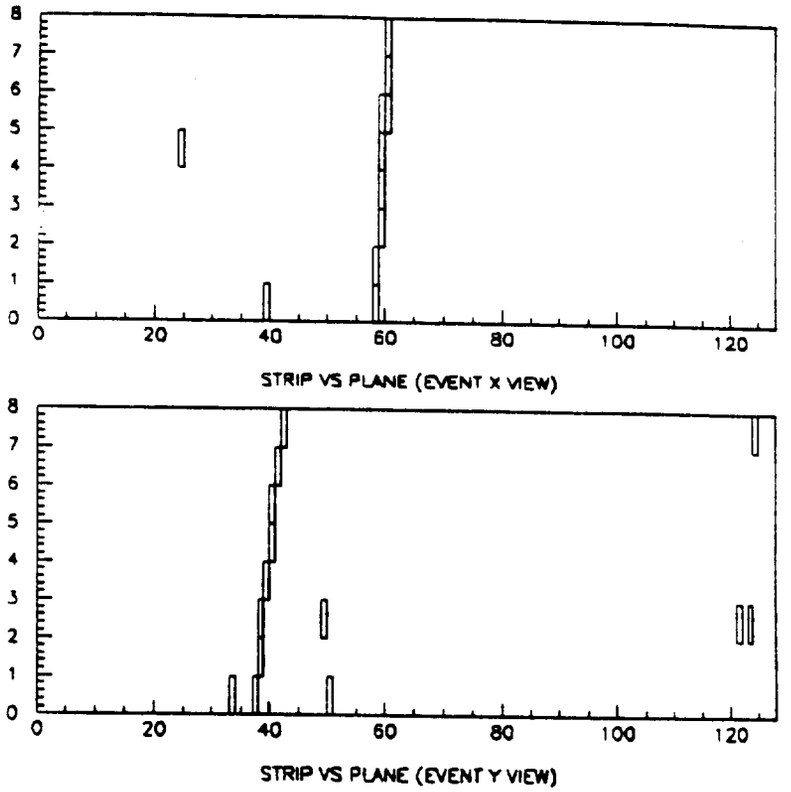

Figure 11 – The imaging capability of the calorimeter: a) a non-interacting particle crossing all the planes; b) an interacting particle initiating an electromagnetic shower .